Hindawi
International Journal of Aerospace Engineering
Volume 2019, Article ID 4135094, 11 pages
https://doi.org/10.1155/2019/4135094

Research Article

An Experimental Characterization on the Acoustic Performance of Forward/Rearward Retraction of a Nose Landing Gear

Yong Liang,[1,2] Kun Zhao,[2] Yingchun Chen,[1] Longjun Zhang,[1,2] and Gareth J. Bennett[3]

[1]*School of Aeronautics, Northwestern Polytechnic University, Xi'an 710072, China*
[2]*Key Laboratory of the Aerodynamic Noise Control, China Aerodynamics Research and Development Centre, Mianyang, Sichuan 612000, China*
[3]*School of Engineering, Trinity College Dublin, University of Dublin, Dublin, D02PN40, Ireland*

Correspondence should be addressed to Kun Zhao; zhaokun@cardc.cn

Received 23 February 2019; Revised 30 April 2019; Accepted 19 May 2019; Published 4 July 2019

Academic Editor: Andre Cavalieri

The modern undercarriage system of a large aircraft normally requires the landing gear to be retractable. The nose landing gear, installed in the front of the fuselage, is retracted either forward or rearward. In the forward/rearward retraction system, the landing gear is normally installed to the trailing/leading side of the bay. When the incoming flow passes the landing gear as well as the bay, the installation that corresponds to the forward/rearward retraction system has a significant impact on the coupling flow and the associated noise of the landing gear and the bay. In this paper, acoustic performance of the forward/rearward retraction of the nose landing gear was discussed based on experiment. The landing gear bay was simplified as a rectangular cavity, and tests were conducted in an aeroacoustics wind tunnel. The cavity oscillation was first analyzed with different incoming speeds. Then, the landing gear model was installed close to the trailing and the leading side of the cavity, respectively. It was observed that installation close to the leading side can help disturb the shear layer so as to suppress the oscillation, while the trailing one can make the landing gear itself produce lower noise. Accordingly, conclusions on the acoustic performance of the forward/rearward retraction of the nose landing gear are made.

1. Introduction

Aircraft noise is emitted by the aircraft or its component during a variety of flight phases such as approach and take-off. To date, it is only second to the road traffic noise in urban areas in terms of its unsociable levels, frequency, and time of occurrence, and it is often at the top of the list in rural areas [1]. Due to the increasing popularity of air travel and the rapid development of aeronautics in the past decades, aircraft noise has become not only an engineering problem but also a political and social issue [2]. Aircraft noise can be fundamentally classified into engine noise and airframe noise. To date, the engine noise has been significantly reduced due to the application of high by-pass ratio configuration, acoustic lining, chevron nozzle lip, etc. [3]. As such, the relative contribution to the total emission from the airframe noise has increased to a new level, and it has become a major concern to the aeronautical engineers.

Airframe noise is generated through the interaction of turbulent flows with solid bodies on the aircraft, major sources of which are the landing gear, slat, flap, etc. The landing gear has a very complex structure, primarily designed to support the entire landing aircraft load when it lands on the ground. In order to facilitate inspection and maintenance, which are crucial to safety, aerodynamic design of the landing gear is not refined, thereby generating much noise when it is directly exposed into the airflow at take-off and approach stages. As such, landing gear noise has been widely investigated in recent decades [4].

Nowadays, the landing gears are conventionally retractable, i.e., when not needed during the flight, the undercarriages will retract into the fuselage and be concealed behind doors. The space for concealing the retractable gears is termed as the landing gear bay. The nose landing gear, which is installed in the front of the fuselage, is retracted either forward or rearward. As illustrated in Figure 1, in

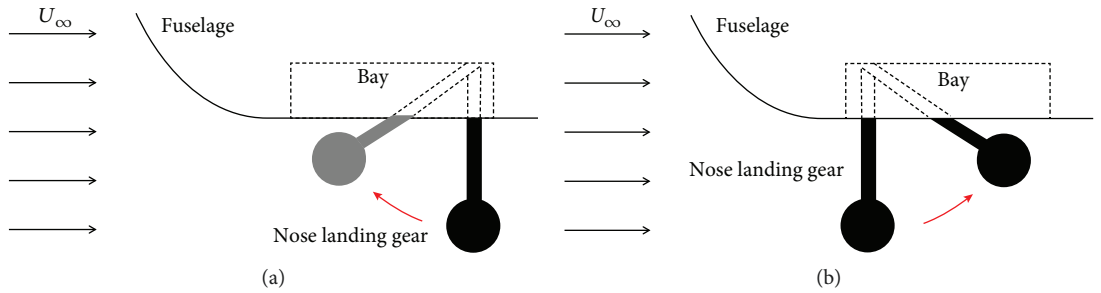

Figure 1: Schematic of the forward/rearward retraction of a nose landing gear: (a) forward retraction; (b) rearward retraction.

the forward/rearward retraction system, the landing gear is normally mounted close to the trailing/leading side of the bay, respectively, retracting to the other side. The forward retraction, as the current mainstream, can be usually found in the aeroplanes manufactured by Boeing and Airbus, e.g., Boeing 777, Airbus 320. By contrast, it is known that some aeroplanes, e.g., Tu 154 from Russia (former Soviet Union), uses the rearward retraction.

When the bay door opens and the landing gear is dropped, the bay itself will play a role as a large cavity, with considerable cavity noise generated. Therefore, the bay has been identified as one of the dominant noise sources related to the landing gear in certain frequency ranges [5]. Additionally, regardless of the two retraction systems, i.e., the frontward and the rearward, turbulent wake of the upstream component will interact with the other downstream, which can be a new indirect noise source. Research on the landing gear bay noise can date back to the 1970s [5, 6], and the cavity oscillation has been identified as the main characteristic of the noise emission. To predict frequencies or the Strouhal number of the oscillation, Rossiter [7] proposed a semiempirical equation based on the experimental data, which has been widely used in the subsequent cavity noise studies [8–11]. As for the noise reduction, a few ideas have been proposed either for the landing gear or for the bay, such as the fairings [12, 13], plasma [14, 15], mesh [16, 17], air curtain [18–21], and upstream mass flow injection [22–24]. Regardless of their technology readiness level (TRL), all of them have been confirmed to be able to achieve noise suppression.

From the brief review above, it is found that though a significant amount of research has been conducted on the landing gear or the bay noise, little work has been made to characterize the different acoustic performance of the forward/rearward retraction. In this paper, the noise of the bay, as well as its assembly with different nose landing gear installation, is discussed, corresponding to forward/rearward retraction. To begin with, the landing gear bay was simplified as a rectangular cavity, and wind tunnel tests were made to characterize its oscillation. Frequencies of the first four Rossiter orders measured from the experiment were compared to the prediction. Then, the nose landing gear model was installed close to the leading and the trailing edges of the cavity, respectively. This allows discussing the interaction between the nose landing gear and the cavity in the two retraction systems. At last, conclusions on the acoustic performance of the forward/rearward retraction of the nose landing gear are made.

2. Experimental Facilities and Instrumentation

2.1. 0.55 m × 0.4 m Low-Speed Aeroacoustic Wind Tunnel. All experiments were conducted in the 0.55 m × 0.4 m aeroacoustic wind tunnel located in China Aerodynamics Research and Development Centre (CARDC). As shown in Figure 2(a), the wind tunnel is driven by a fan with the maximum power to be 130 kW. In the test section, the size of the nozzle outlet is 0.55 m × 0.4 m, and the main flow speed can be up to 100 m/s. The test section is equipped with a fully anechoic chamber (3 m × 3.7 m × 5.20 m), with the cut-off frequency to be 100 Hz. The background noise is less than 75-80 dB, and the turbulence intensity of the core area is ≤0.05%. In addition, one collector is installed opposite to the nozzle, with an open size of 0.72 m × 0.72 m. The collector allows the main flow air to return to the wind tunnel loop. Pictures of the wind tunnel full view and the anechoic chamber are provided in Figures 2(b) and 2(c).

2.2. Acoustic Measurement Instrument. The acoustic measurement was conducted through a microphone array and a far-field microphone arc, utilized for noise localization and directivity analysis, respectively. Setup of the microphone is shown in Figure 3(a). Details of the setup are provided in Figure 3(b); it is shown that the distance from the measurement plane to the microphone array was 930 mm. The height of the arc, i.e., from the bottom microphone to the endplate, was 80 mm, making the bottom of the arc flush with the top edge of the landing gear model.

All microphones are 1/4 inch G.R.A.S. 46BE type, with a dynamic range to be 35 dBA-160 dB. The sensitivity of the microphone is 4 mV/Pa. Each microphone has been calibrated with a 42AB calibrator at 1 kHz. For data acquisition, the microphones were connected to a NI PXIe-4499 data acquisition card, and the sampling frequency and time were set to be 51.2 kHz and 10 s. The microphone array consists of 70 microphones, mounted in an open grid with a spiral pattern. The coordinates in detail are described in Figure 4(a). To avoid the disturbance from the main flow, each microphone was equipped with a windproof cap, shown in Figure 4(b). The microphone arc, used for far-field directivity measurement, was installed along with the microphone array. There were 9 microphones, spaced equally from -90°

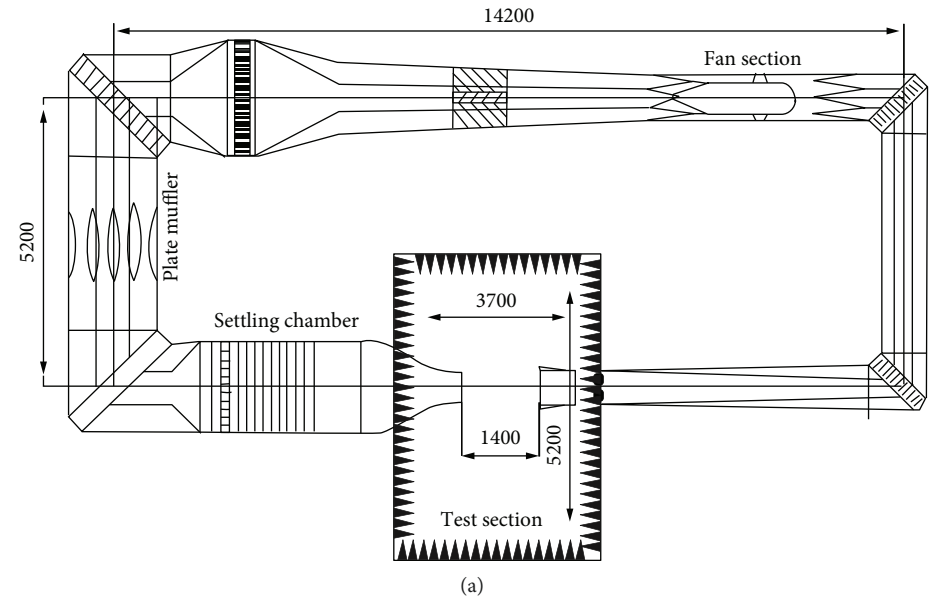

(a)

(b)

(c)

Figure 2: 0.55 m × 0.4 m aeroacoustic wind tunnel in CARDC: (a) plan; (b) full view; (c) anechoic chamber with the main flow nozzle outlet.

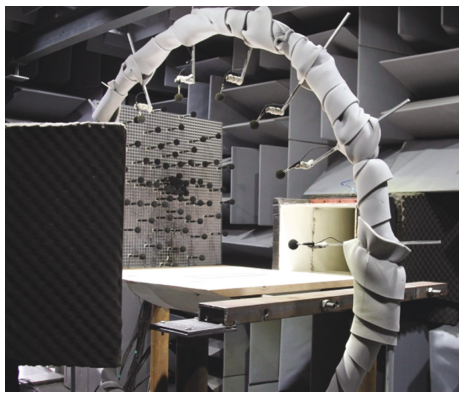

(a)

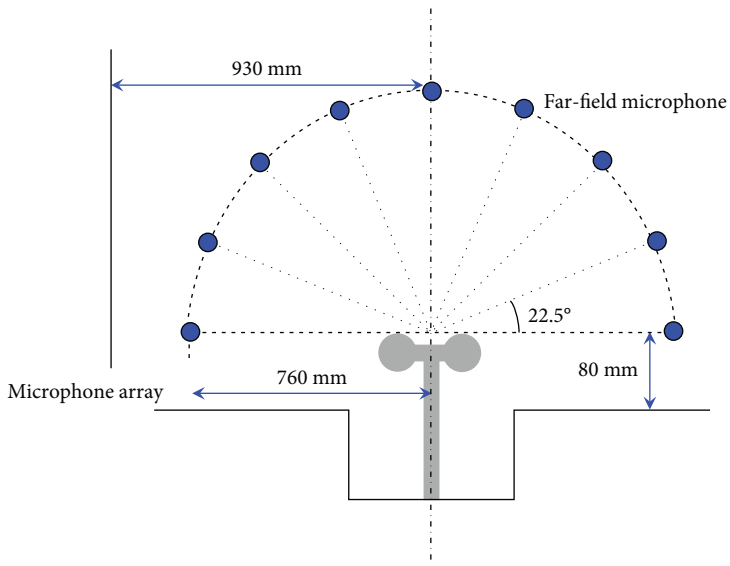

(b)

Figure 3: Acoustic measurement setup: (a) view of the installation; (b) schematic of the installation.

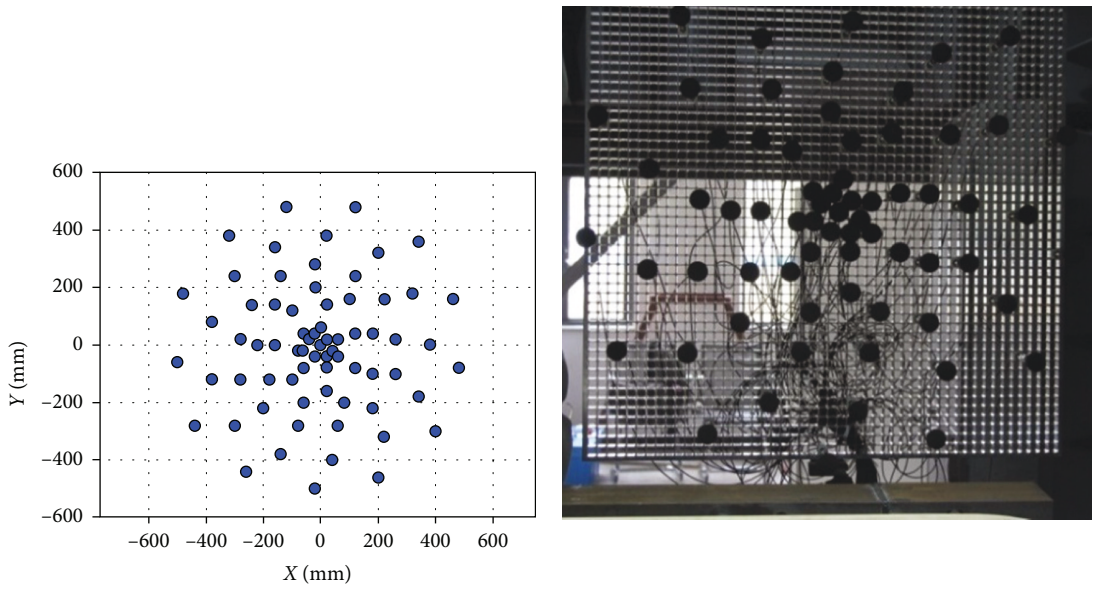

Figure 4: Microphone array used for the noise localization: (a) pattern of the microphone array; (b) front view of the microphone array.

Table 1: Test matrix.

Case no.	Cavity dimension ($l \times h \times w$)	U_∞	Ma	Landing gear position	Noise reduction rig
1	—	60 m/s	0.18	—	—
2	232 mm × 120 mm × 116 mm	40 m/s	0.12	—	—
3	232 mm × 120 mm × 116 mm	50 m/s	0.15	—	—
4	232 mm × 120 mm × 116 mm	60 m/s	0.18	—	—
5	232 mm × 120 mm × 116 mm	60 m/s	0.18	P1	—
6	232 mm × 120 mm × 116 mm	60 m/s	0.18	P2	—

to 90° with an interval of 22.5°. The diameter of the arc geometry was 2000 mm; however, each far-field microphone was mounted in an inner circle with a radius of 760 mm.

2.3. Test Programme and Model Setup. In this paper, a number of different configurations were tested as a parametric study to analyze the noise characteristics. All cases are shown in the test matrix in Table 1. For different purposes, those cases can be classified into two groups. Group I includes Cases No. 2-4, which can be used to discuss the effects from different main flow speeds on the cavity noise. The configuration is illustrated in Figure 5, the distance from the cavity leading edge to the nozzle outlet is 180 mm, and the total dimension of the test platform is 1200 mm. In the test, U_∞ was controlled to be 40 m/s, 50 m/s, and 60 m/s, respectively.

Group II includes Cases No. 1 and 4-6, used to characterize the noise of the landing gear model when it is installed at different position of the cavity, corresponding to the forward/rearward retraction system. As shown in Figure 6(a), the model used was a simplified nose landing gear with two wheels assembled. The model was manufactured with stainless steel, polished to delay the transition. It was installed close to the leading and trailing edges of the cavity, respectively, with a distance of 8 mm. Hereinafter, the two positions were termed as P1 and P2, illustrated in Figure 6(b). Note that Case 1 was used to characterize the background noise, i.e., there is no cavity nor landing gear model inside.

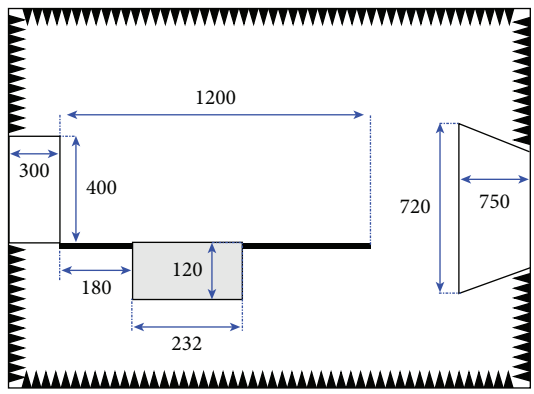

Figure 5: Test setup for the cavity noise characterization with a landing gear model (in mm).

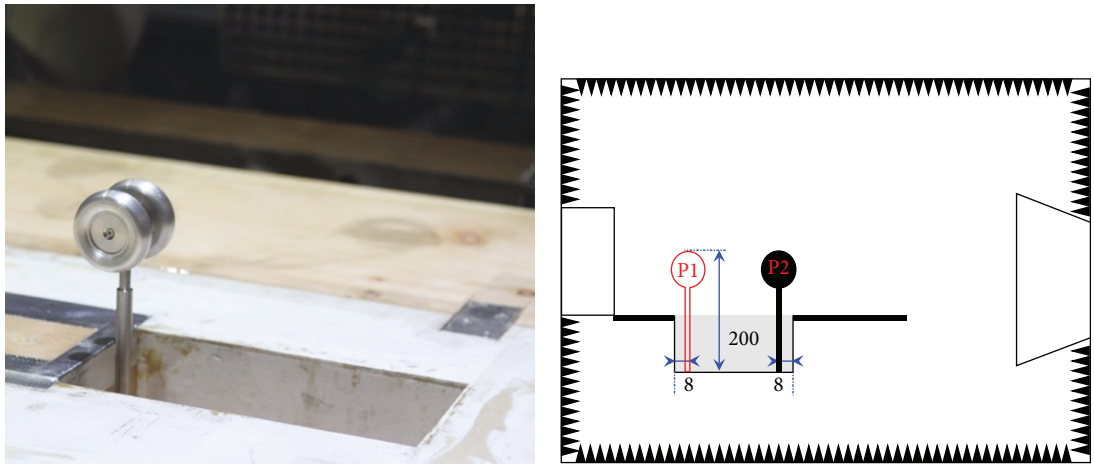

(a) (b)

Figure 6: Test setup of the cavity noise characterization with a landing gear model: (a) landing gear model; (b) schematic for the configuration (in mm).

3. Results and Discussion

In this section, test results are discussed in detail. As mentioned above, each subsection will concentrate on one parameter that has effects on the noise emission, e.g., U_∞ and assembly position of the landing gear. Note that the different assembly position corresponds to the forward and the rearward retraction system.

3.1. Speed of the Incoming Flow. The incoming flow speed, i.e., U_∞, is one of the most important factors that dominate the noise characteristics of a cavity. Figure 7 illustrates the experimental results in A-weighted OASPL (overall sound pressure level) of Cases 4-2 from those far-field microphones in the arc, and the polar system is used. Note that the azimuth shows the angle deviating from the vertical direction, denoted as φ. As such, when $\varphi = 0°$, it refers to the microphone that is on the right top of the cavity. Obviously, for this rig, the range of φ is [-90°, 90°]. As expected, OASPL is observed to increase with U_∞. For each U_∞, it is observed that with the change of φ, OASPL shows a directivity distribution. More specifically, OASPL peaks at ±67.5°, which means from $\varphi = 0°$ to the horizontal direction ($\varphi = \pm 90°$), OASPL increases first till $\varphi = \pm 67.5°$ and then decreases.

Apart from directivity, more characteristics can be found in the spectra in Figure 8. The data here were obtained from the microphone $\varphi = 0°$, and it is used in the remainder of this paper as well. Note that the spectra here have been also A-weighted to highlight the frequency range of interest. As shown in Figure 8, in addition to the SPL level, the tones of each case show up at different frequencies when U_∞ varies. Those tones are the results of the high amplitude feedback resonance induced by the shear layer oscillation. As depicted in Figure 9, due to the separation of the upstream edge, an instability within the turbulent shear layer will develop and spans the length of the cavity. When it reattaches the trailing edge, the impingement region will become the primary acoustic sources. As such,

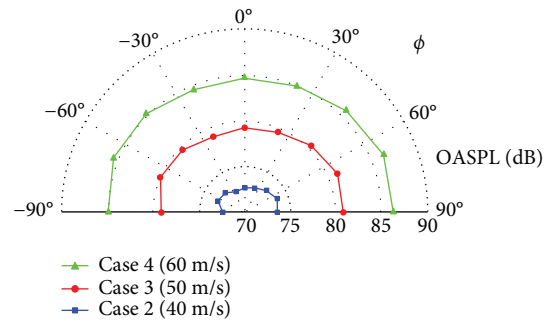

Figure 7: A-weighted directivity performance of the cavity at different main flow speeds.

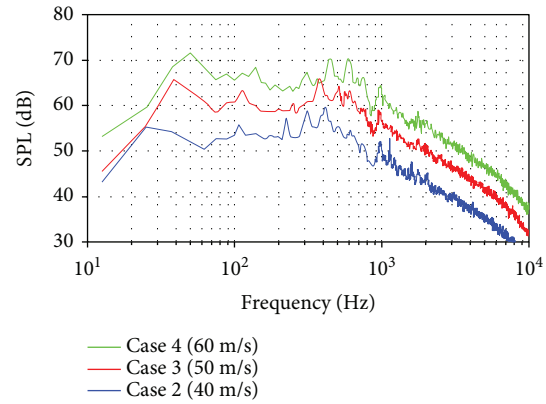

Figure 8: A-weighted SPL spectra of the cavity noise at different flow speeds.

the leading and the trailing edges are also referred to as the separation edge and the impingement edge hereinafter. The acoustic waves propagate to all directions including the upstream. As it reattaches the separation edge, the incident acoustic waves act as the perturbation and trigger the

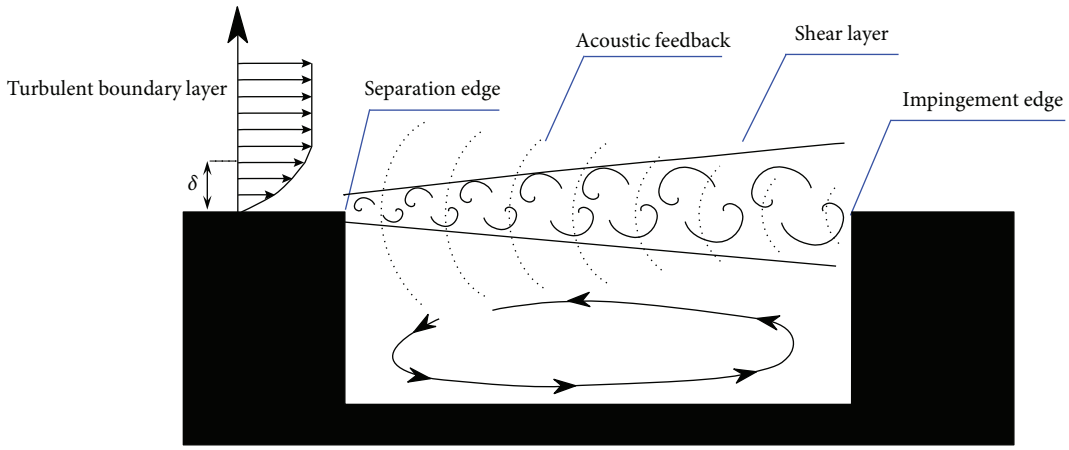

Figure 9: Schematic of the flow-induced cavity resonance.

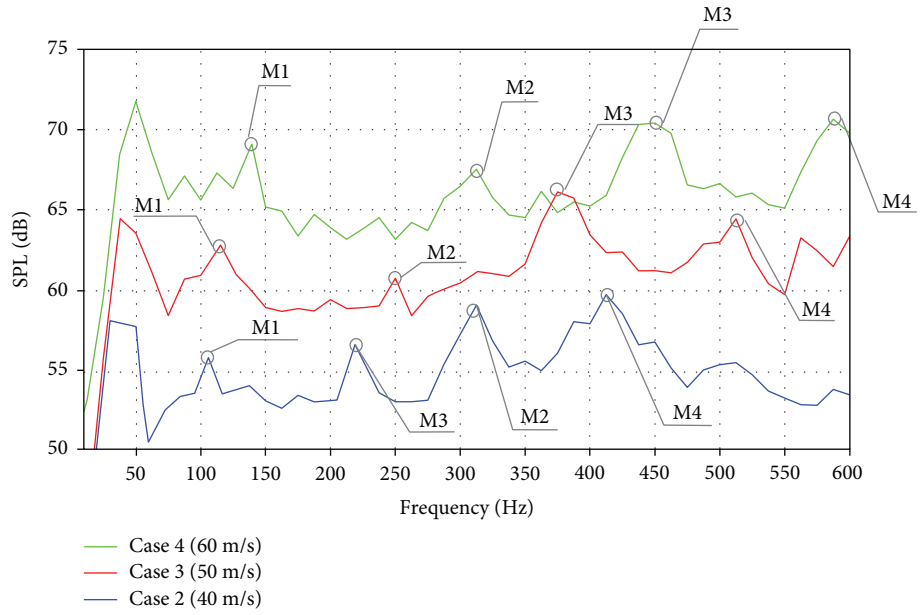

Figure 10: Shear layer modes of the test cases.

generation of another instabilities with noise at different frequencies generated, i.e., the Rossiter modes.

Many studies [6, 8, 9] have been conducted to predict the frequencies of such shear layer modes. As mentioned in Section 1, the semiempirical equation based on the experimental data has been popularly used. This equation was proposed by Rossiter [7], written as

$$f = \frac{U_\infty}{l} \frac{n - \alpha}{Ma + 1/\kappa}, \quad (1)$$

where n is the order of the shear layer mode; Ma is the Mach number of the mainflow. κ and α are the two important coefficients. κ is the ratio between the convection speed of the vertical structures in the shear layer and the main flow speed. α is the phase delay between the hydrodynamic forcing and the acoustic feedback. In this paper, different values of κ were tested from 0.4 to 0.7 and the best fit was found to be 0.67, which enables equation (1) to well predict each modes, discussed later in this section. As for α, Chatellier et al. [25] argued that the phase delay is not necessary and for those cases with the speed of the flow to be much lower than the sound. Therefore, in this study, α is set to be zero. Figure 10 is a zoom-in of the spectra in Figure 8, which illustrates the first four modes of each cases acquired from the experimental data. M1 means the first mode, M2 the second, and so on. These tones were identified with the help of equation (1), discussed in later in this section.

The values from the prediction and the experiment of the first four modes are listed in Table 2. To clearly illustrate the trend, a diagram is also given in Figure 11, which is designed as the Strouhal number against the Mach number. It is observed that the values predicted for the first four modes are in good agreement with the experiment. Therefore, we

Table 2: Modes of the cavity noise.

		Mode I	Mode I	Mode III	Mode IV
Case 4	Pre	150.8 Hz	301.6 Hz	452.4 Hz	603.2 Hz
	Exp	141.6 Hz	318.7 Hz	450.0 Hz	583.5 Hz
Case 3	Pre	127.9 Hz	255.7 Hz	383.6 Hz	511.5 Hz
	Exp	119.4 Hz	250.0 Hz	374.3 Hz	521.3 Hz
Case 2	Pre	104.1 Hz	208.2 Hz	312.3 Hz	416.4 Hz
	Exp	107.3 Hz	217.5 Hz	319.2 Hz	415.4 Hz

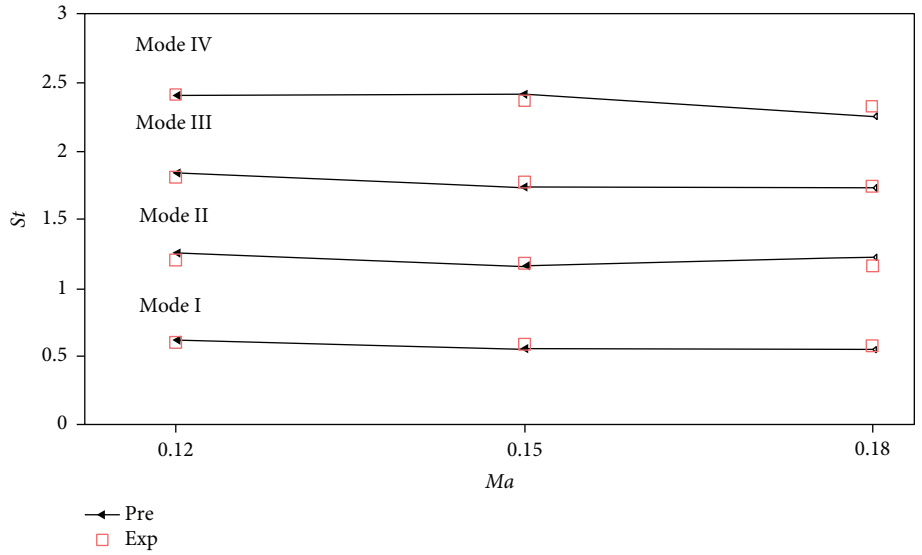

Figure 11: Comparison between the prediction and experimental results on the acoustic modes of the test cases as a function of the Mach number.

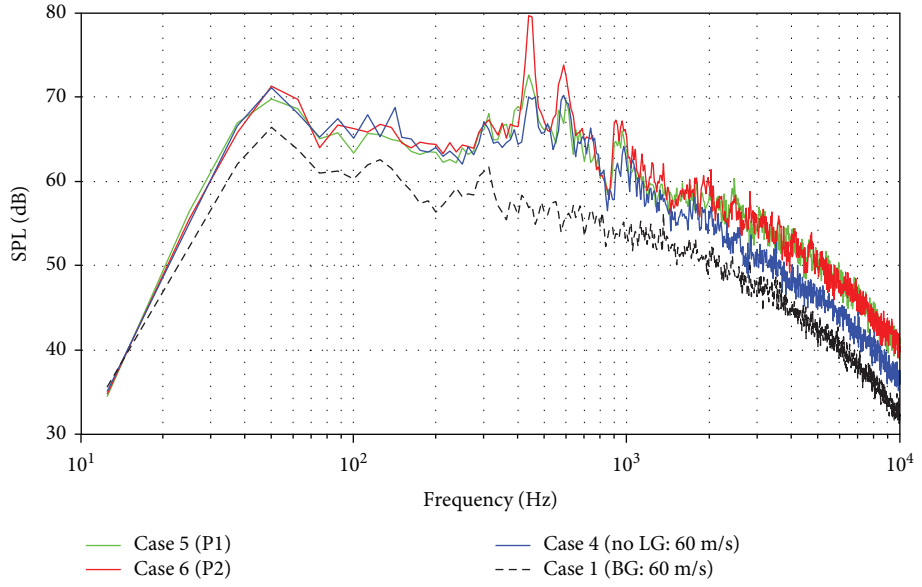

Figure 12: A-weighted spectra for those cases related to the landing gear assembly position.

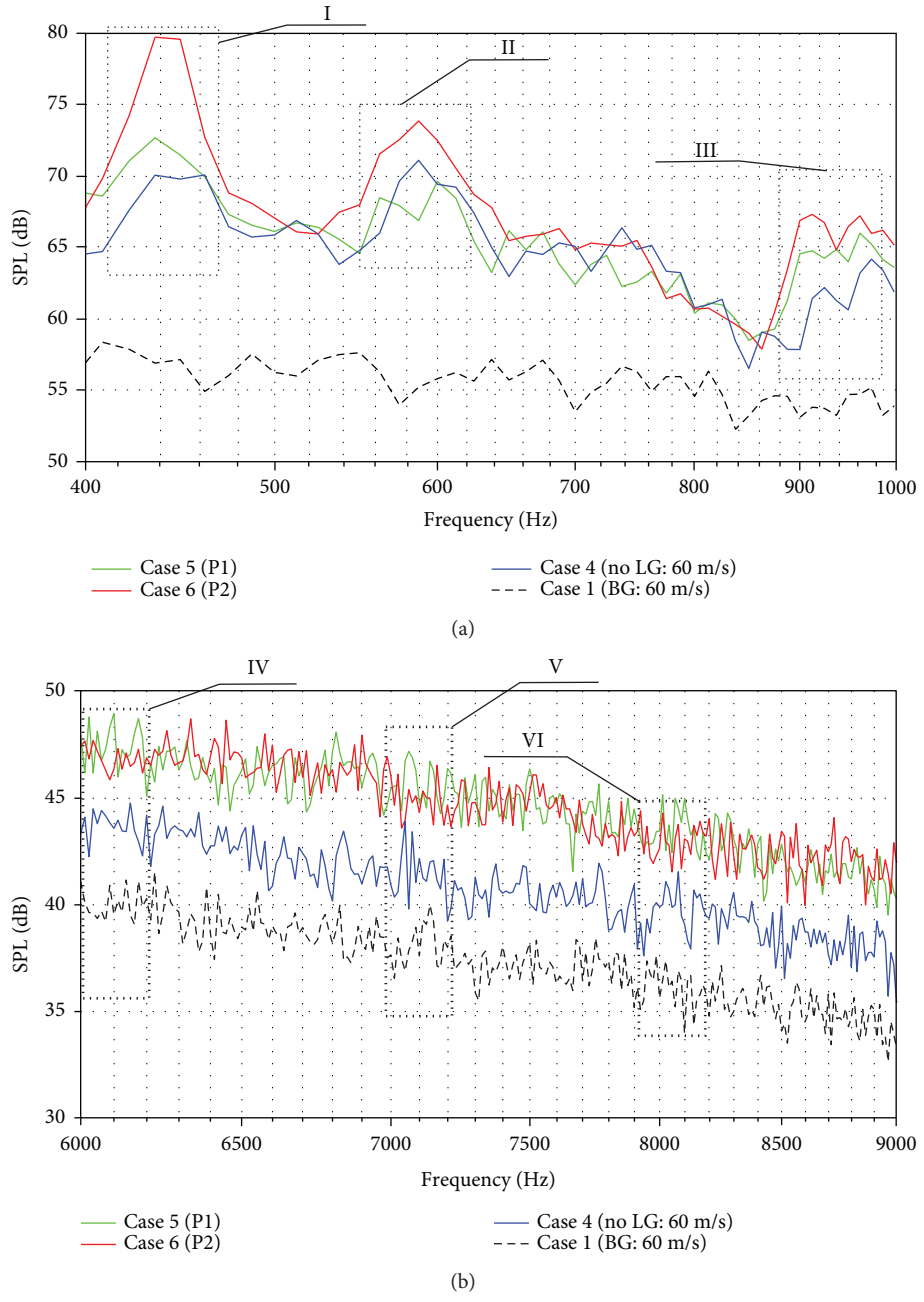

FIGURE 13: Narrowband A-weighted spectra in different frequency ranges: (a) 400 Hz-1000 Hz; (b) 6000-9000 Hz.

can conclude that through the selection of the κ and α, the semiempirical equation of Rossiter [7] can be used to well capture the modes of the cavity resonance.

3.2. Assembly Position of the Landing Gear. Assembly position of the landing gear related to the bay, which corresponds to the forward/rearward retraction, can be an important factor that affects the noise characteristics of the entire undercarriage system. In order to evaluate the acoustic performance, the landing gear model was attached on the leading and the trailing side of the cavity, respectively, i.e., P1 and P2.

The A-weighted spectra of each case related to the installation of the landing gear model are presented in Figure 12, including Cases 1 and 4-6. More specifically, Cases 5 and 6 refer to those configurations with the landing gear model installed upstream (P1) and downstream (P2). Cases 4 and 1 are the cavity only (benchmark test) and the background noise with only the main flow blowing. Note that U_∞ in all cases here is 60 m/s. It is observed that in Figure 12, the installation of the landing gear model contributes to the increase of SPL in almost all frequencies. Obviously, this is because as a bluff body, the landing gear model can induce flow separation so as to make much noise. However, it is

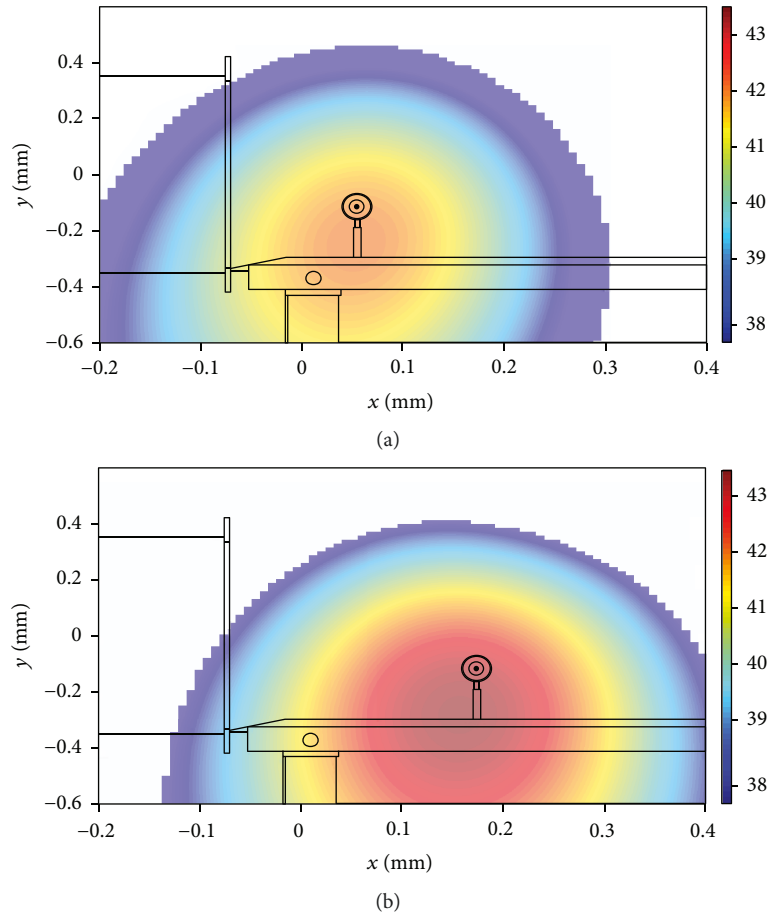

Figure 14: Beamforming results at 900 Hz: (a) Case 7; (b) Case 8.

found that in some modes of the shear layer oscillation, SPL reduces, e.g., 1st and 2nd modes discussed in Section 3.1. The explanation can be the perturbation that the landing gear model brings into the shear layer of the separation edge. To be more specific, the cavity oscillation is induced due to the impinging of the shear layer on the trailing edge, depicted in detail in Figure 9. However, when the landing gear model exists, part of the shear layer from the separation edge will impinge on its strut, regardless of the model installation. In other words, the mechanism of the cavity oscillation will be disturbed. Note that this disturbance only affects the cavity flow field where the landing gear model stays, i.e., in the middle; the flow field in the side will not be affected. This can explain why SPL in some modes reduces but still exists.

When the turbulent shear layer, instead of the laminar incoming flow, impinges on the landing gear installed at different locations, the acoustic performance of the landing gear requires analysis as well. Figure 13 includes the narrowband spectra zoomed in different frequency ranges. Figure 13(a) illustrates the low-frequency band from 400 Hz to 1000 Hz, showing that in some frequencies the SPL of Case 6 is higher than case 5, e.g., those that are highlighted by the dashed blocks I-III. While in the high-frequency range, for example, 6000 Hz to 9000 Hz in Figure 13(b), Case 5 is higher than Case 6 in some frequencies such as the dashed blocks IV-VI.

To further explain the acoustic performance, noise source localization is used in this paper, achieved from the microphone array based on beamforming algorithm. As depicted in Figures 14 and 15, SPL contour at 900 Hz and 6100 Hz is presented. 900 Hz was chosen as the frequency of interest in the low-frequency range to achieve an acceptable beamwidth for analysis. Note that in those images at the same frequency, range of the colour bar is managed to be identical so that SPL can be compared. From the comparison between Figures 14(a) and 14(b), it is observed that at 900 Hz, regardless of the landing gear installation, noise is mainly produced from the cavity, which is consistent with the information reported in the spectra in Figure 12. In addition, Case 8 shows to be noisier than Case 7. By contrast, at 6100 Hz the results are opposite, shown in Figures 15(a) and 15(b). These results are also in good agreement with what the spectra illustrate in Figure 12. Additionally, more important information can be observed from where the peak of the contour is, i.e., the wheel. Therefore, from Figure 14, it is found that the noise at 900 Hz is mainly from the cavity side. At 6100 Hz, the peak shows up around the wheel and the upper side of the strut, which means that the flow separation from the landing gear itself dominates the noise generation in this frequency. As such, when the landing gear is attached upstream in P1, the incoming flow is relatively stronger than P2 and accordingly the flow separation noise is higher.

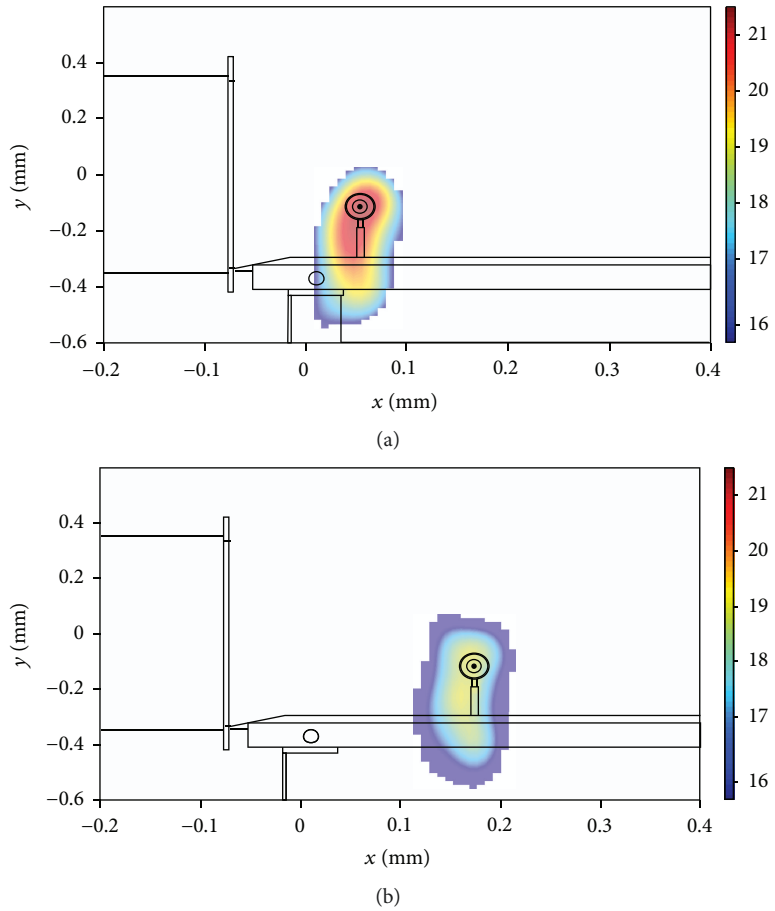

Figure 15: Beamforming results at 6100 Hz: (a) Case 7; (b) Case 8.

In conclusion, no matter where the landing gear is installed, it can disturb the shear layer oscillation when the landing gear is attached. Between P1 and P2, when the landing gear is attached upstream, it can benefit the reduction of the impinging noise to the strut from the shear flow; if attached to the trailing side of the bay, the flow separation noise will be less.

4. Summary

In this paper, acoustic characteristics of the different landing gear and bay assemblies were discussed, corresponding to the forward/rearward retraction. The bay was simplified into a rectangular cavity, and a parametric study was conducted. For the cavity noise, its characteristics related to the speed of the incoming flow was first analyzed through three cases. First of all, from the OASPL achieved from the far-field microphones in the arc, it was observed that the cavity shows an obvious sound directivity. Then, the cavity resonance was discussed in detail through the first four modes of each case. The frequencies measured from the experiment were compared to the values that are calculated using a semiempirical equation. The results showed that a good agreement can be attained when the two coefficients, i.e., κ and α, are managed well. Effects on the noise characteristics of the landing gear relative position to the cavity were also discussed, which corresponds to the forward/rearward retraction system. A landing gear model was installed close to the leading and the trailing edges of the cavity, respectively. From the experimental measurement, it is found, as expected, that the landing gear model can bring in extra noise emission. Furthermore, when it is installed close to the leading side, it can disturb the shear layer originating from the separation edge so as to reduce the oscillation noise. By contrast, when it is installed close to the trailing side of the cavity, the oscillation cannot be mitigated but the landing gear itself will have less noise production.

Data Availability

The experiment data used to support the findings of this study are included within the article.

Conflicts of Interest

The authors declare that there is no conflict of interest regarding the publication of this paper.

Acknowledgments

This research was supported by the National Key R&D Program of China (Grant No. 2017YFE0123300).

References

[1] M. J. T. Smith, *Aircraft Noise*, Cambridge University Press, 1989.

[2] P. Argüelles, M. Bischoff, P. Busquin, B. A. C. Droste, R. H. Evans, and W. Kröll, "European aeronautics: a vision for 2020," *Report of the Group of Personalities, The European Commission*, vol. 12, 2001.

[3] D. Casalino, F. Diozzi, R. Sannino, and A. Paonessa, "Aircraft noise reduction technologies: A bibliographic review," *Aerospace Science and Technology*, vol. 12, no. 1, pp. 1–17, 2008.

[4] W. Dobrzynski, "Almost 40 years of airframe noise research: what did we achieve?," *Journal of Aircraft*, vol. 47, no. 2, pp. 353–367, 2010.

[5] H. H. Heller and W. M. Dobrzynski, "Sound radiation from aircraft wheel-well/landing-gear configurations," *Journal of Aircraft*, vol. 14, no. 8, pp. 768–774, 1977.

[6] D. B. Bliss and R. E. Hayden, "Landing gear and cavity noise prediction," Tech. Rep. NASA-CR-2714, Cambridge, MA, USA, 1976.

[7] J. Rossiter, *Wind tunnel experiments on the flow over rectangular cavities at subsonic and transonic speeds*, Ministry of Aviation; Royal Aircraft Establishment; RAE Farnborough, 1964.

[8] E. Neri, J. Kennedy, and G. J. Bennett, "Bay cavity noise for full-scale nose landing gear: a comparison between experimental and numerical results," *Aerospace Science and Technology*, vol. 72, pp. 278–291, 2018.

[9] L. Cattafesta, F. Alvi, D. Williams, and C. Rowley, "Review of active control of flow-induced cavity oscillations (invited)," in *33rd AIAA Fluid Dynamics Conference and Exhibit*, Orlando, FL, USA, June 2003.

[10] T. Handa, K. Tanigawa, Y. Kihara, H. Miyachi, and H. Kakuno, "Frequencies of transverse and longitudinal oscillations in supersonic cavity flows," *International Journal of Aerospace Engineering*, vol. 2015, Article ID 751029, 7 pages, 2015.

[11] H. Yokoyama, H. Odawara, and A. Iida, "Effects of freestream turbulence on cavity tone and sound source," *International Journal of Aerospace Engineering*, vol. 2016, Article ID 7347106, 16 pages, 2016.

[12] W. Dobrzynski, L. Chow, P. Guion, and D. Shiells, "Research into landing gear airframe noise reduction," in *8th AIAA/-CEAS Aeroacoustics Conference & Exhibit*, Breckenridge, CO, USA, June 2002.

[13] K. Boorsma, X. Zhang, N. Molin, and L. C. Chow, "Bluff body noise control using perforated fairings," *AIAA Journal*, vol. 47, no. 1, pp. 33–43, 2009.

[14] F. Thomas, A. Kozlov, and T. Corke, "Plasma actuators for landing gear noise reduction," in *11th AIAA/CEAS Aeroacoustics Conference*, Monterey, CA, USA, May 2005.

[15] X. Huang, X. Zhang, and Y. Li, "Broadband flow-induced sound control using plasma actuators," *Journal of Sound and Vibration*, vol. 329, no. 13, pp. 2477–2489, 2010.

[16] O. Stefan, S. Constantin, M. Nicolas, and P. Jean-Francois, "Reduction of landing gear noise using meshes," in *16th AIAA/CEAS Aeroacoustics Conference*, Stockholm, Sweden, June 2006.

[17] P. N. Okolo, K. Zhao, J. Kennedy, and G. J. Bennett, "Mesh screen application for noise reduction of landing gear strut," in *22nd AIAA/CEAS Aeroacoustics Conference*, Lyon, France, May 2016.

[18] S. Oerlemans and A. C. Bruin, "Reduction of landing gear noise using an air curtain," in *Proceedings of the 5th AIAA/CEAS Aeroacoustics Conference*, pp. 2009–2403, Miami, FL, USA, May 2009.

[19] K. Zhao, X. Yang, P. N. Okolo, W. Zhang, and G. J. Bennett, "Use of plane jet for flow-induced noise reduction of tandem rods," *Chinese Physics B*, vol. 25, no. 6, article 064301, 2016.

[20] K. Zhao, X. Yang, P. N. Okolo, Z. Wu, and G. J. Bennett, "Use of dual planar jets for the reduction of flow-induced noise," *AIP Advances*, vol. 7, no. 2, article 025312, 2017.

[21] K. Zhao, S. Alimohammadi, P. N. Okolo, J. Kennedy, and G. J. Bennett, "Aerodynamic noise reduction using dual-jet planar air curtains," *Journal of Sound and Vibration*, vol. 432, pp. 192–212, 2018.

[22] W. Li, "Suppression of supersonic cavity oscillations using pulsed upstream mass injection," *International Journal of Aerospace Engineering*, vol. 2016, Article ID 6702385, 6 pages, 2016.

[23] S. Arunajatesan, C. Kannepalli, N. Sinha et al., "Suppression of cavity loads using leading-edge blowing," *AIAA Journal*, vol. 47, no. 5, pp. 1132–1144, 2009.

[24] G. J. Bennett, P. N. Okolo, K. Zhao, J. Philo, Y. Guan, and S. C. Morris, "Cavity resonance suppression using fluidic spoilers," *AIAA Journal*, vol. 57, no. 2, pp. 706–719, 2019.

[25] L. Chatellier, J. Laumonier, and Y. Gervais, "Theoretical and experimental investigations of low Mach number turbulent cavity flows," *Experiments in Fluids*, vol. 36, no. 5, pp. 728–740, 2004.